02 83 01

Nuclear Physics A405 (1983) 313–347

THE (^{14}C, ^{14}O) REACTION CONSIDERED AS SIMULTANEOUS PAIR-EXCHANGE OR DOUBLE-CHARGE-EXCHANGE PROCESSES

D. R. BES†, O. DRAGÚN and E. E. MAQUEDA†

Departamento de Física, Comisión Nacional de Energía Atómica, 1429 Buenos Aires, Argentina

Received 19 November 1982

Abstract: Pair-exchange or double-charge-exchange reactions are studied from the point of view of one-step processes. Two possible mechanisms are analyzed, involving either the simultaneous exchange of a dineutron and a diproton between the target and the projectile or the simultaneous transformation of the charge of the dinucleon in each system. Although the formalism is explicitly developed for the (^{14}C, ^{14}O) reaction, its extension to other projectiles is straightforward. The possibility of populating collective states which otherwise are very difficult to attain is stressed. Application is made to the cases of the ^{208}Po(^{14}C, ^{14}O)^{208}Pb and ^{40}Ca(^{14}C, ^{14}O)^{40}Ar reactions.

1. Introduction

So far, the nuclear structure knowledge which has been obtained from peripheral heavy ion reactions has been comparatively meagre, in relation to the vast amount produced by the light ion reactions. Nevertheless, there are a number of processes in which heavy ions could yield rather unique information, such as multiple Coulomb excitation and the transfer of particles from excited states, multiple pair transfer processes (nuclear Josephson effect), etc. Among these processes we may include the present type of reactions, which involve either the simultaneous exchange of a dineutron and a diproton or the exchange of two units of charge between target and projectile. Such processes should be sensitive to the nucleon-nucleon residual correlations. They can also be considered to be a complement of the (π^+, π^-) [ref. [1])] pion double-charge-exchange reactions.

These reactions may specifically populate certain collective states some of which have been difficult to attain by other experimental means.

We shall restrict our present study to the (^{14}C, ^{14}O) reaction, although the formalism can be straightforwardly modified for its application to different projectiles. This reaction (^{14}C, ^{14}O) has presently been performed on ^{40}Ca with sizeable cross sections [2]).

† Fellow of the CONICET, Argentina.

A general derivation of the formalism is given in sect. 2, and in sect. 3 some macroscopic and microscopic features of the results are discussed. The calculations are mainly performed for the case of the reaction $^{208}Po(^{14}C, ^{14}O)^{208}Pb$ at the laboratory energy of 250 MeV. This reaction was chosen because of the interest of the nuclear structure in the lead region, although other targets can be similarly considered. In particular, in subsect. 3.5 a calculation for the reaction on ^{40}Ca at $E_{lab} = 51$ MeV is presented, aimed at a comparison with the experimental observations.

2. Discussion of the reaction mechanism

2.1. GENERAL ASSUMPTIONS

If the process is supposed to take place in a single step it can be produced by terms of Wigner and Heisenberg type of the residual effective interaction. For the first type, there is a simultaneous diproton pick-up and a dineutron stripping. Namely, a diproton belonging to the target A is transferred to the ejectile b while at the same time a dineutron from the projectile a is captured by the residual system B (see fig. 1a). In the Heisenberg type, the effective interaction transforms a diproton into a dineutron in the target, while simultaneously a dineutron becomes a diproton in the projectile (see fig. 1b).

In the usual charge-exchange reactions, where a proton of the projectile is transformed into a neutron in the ejectile, more attention is paid to the Heisenberg process. This is partly due to the $\sqrt{T}$ collective enhancement in nuclei with a neutron excess T. We do not expect these collective effects to appear in (^{14}C, ^{14}O) reactions, since the target diproton should transfer into occupied neutron states. Not only there is no relative enhancement, but moreover, we do not have an indication of the relative size and sign of the "Wigner" and "Heisenberg" terms in the effective four-body force which is responsible for the direct pair exchange†. Therefore, in the following, both types of processes will be treated separately, although the corresponding amplitudes should add coherently. Some predicted results are common to both mechanisms and thus are expected to remain valid when the proper linear combination of the two amplitudes will be added. In the present paper we do not attempt to find out which is this linear combination.

† The relative motion of the two dinucleons may be described by wave functions having a sizeable overlap between initial and final states. Therefore, the Wigner term of a two-body interaction yields a nonvanishing matrix element between states differing in the wave function of the c.m. of the dinucleons. On the contrary, the Heisenberg term of a two-body interaction gives vanishing matrix elements, since at most the isospin projection of a single neutron and a single proton may be simultaneously changed. (We are grateful to Prof. F. Brieva for a clarifying discussion on the point.) However, the effective interaction takes into account the effects of other channels (like those involving two successive processes) which may appear as due to an effective four-body Heisenberg term within a one-step description.

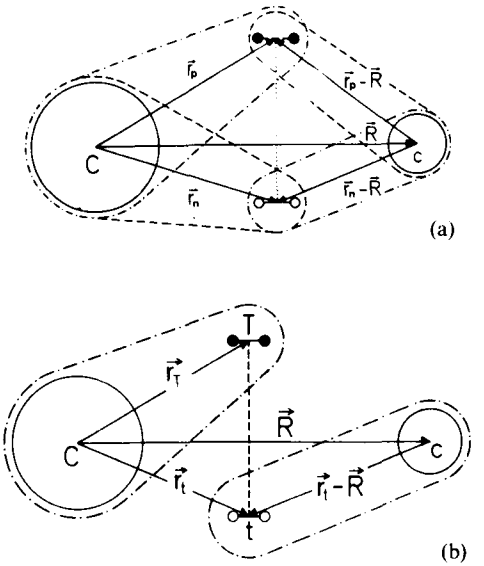

Fig. 1. Schematic representation of the reaction and coordinate systems. (a) Wigner and (b) Heisenberg process. The entrance channel has a target formed by a core C plus a diproton and a projectile formed by a core c plus a dineutron. Dot-dashed lines circle each colliding nuclear system. In the Wigner case dashed lines circle the systems in the exit channel. In the Heisenberg case they are spatially the same as in the entrance channel.

Within the DWBA the reaction amplitude is given by

$$T = \int \chi_{bB}^{(-)} \langle b, B|V|a, A\rangle \chi_{aA}^{(+)} d\boldsymbol{r}_b d\boldsymbol{r}_a, \tag{1}$$

where χ_{aA} and χ_{bB} stand for the distorted wave solutions of the incoming and outgoing optical model potential.

A number of assumptions will be made in order to derive expressions for the form factors $\langle bB|V|aA\rangle$:

(a) The interaction which is responsible for the reaction takes place between the centre of mass (c.m.) of the transferred or transformed dinucleons, i.e. $V = V(|\boldsymbol{r}_n - \boldsymbol{r}_p|)$ in the Wigner process or $V = V(|\boldsymbol{r}_T - \boldsymbol{r}_t|)$ in the Heisenberg process.

(b) The distance R between the c.m. of the heavier core C and the c.m. of the lighter core c is the radial variable entering in the form factor, and in the incident and outgoing distorted waves. This is equivalent to a no-recoil approximation.

(c) The interaction acts only along a narrow cylinder around the axis $\boldsymbol{R}$ passing through the centre of mass of the two cores C and c, i.e. $V(|\boldsymbol{r}_n - \boldsymbol{r}_p|) = r_n^{-2} r_p^{-2} V(|\boldsymbol{r}_n - \boldsymbol{r}_p|)\delta(\Omega_n - \Omega_R)\delta(\Omega_p - \Omega_R)$ or the equivalent expression

for the Heisenberg process. This assumption provides a simple framework in order to evaluate an otherwise difficult integral: not only is it a six-dimensional integral, but also the wave functions corresponding to the c.m. of the dinucleons in the lighter systems are centered at a different origin from those of the heavier systems †.

(d) The interaction has zero range, i.e. $V(r) = V_0\delta(r)$.

We must note that these assumptions are common to many heavy ion calculations. Without loss of generality, we consider only even-even targets A.

2.2. WIGNER PROCESSES

In the case of Wigner processes, the following form factor is obtained (see appendix A) applying assumptions (a) to (d):

$$\begin{aligned}
&\langle \mathrm{b} \equiv {}^{14}\mathrm{O(g.s.)};\ \mathrm{B}(JM)|V(\boldsymbol{r}_\mathrm{n}-\boldsymbol{r}_\mathrm{p})|\mathrm{A(g.s.)};\ \mathrm{a} \equiv {}^{14}\mathrm{C(g.s.)}\rangle \\
&\quad = V_0^{\mathrm{W}} \frac{i^J}{4\pi^{\frac{1}{2}}\sqrt{(2J+1)}} Y^*_{JM}(\Omega_R) \\
&\qquad \times \sum_{\substack{n_\mathrm{n}N_\mathrm{n}n'_\mathrm{n}S_\mathrm{n}L_\mathrm{n}\bar{L}_\mathrm{n} \\ n_\mathrm{p}N_\mathrm{p}n'_\mathrm{p}S_\mathrm{p}L_\mathrm{p}\bar{L}_\mathrm{p}}} I(N_\mathrm{n}, \bar{L}_\mathrm{n}; N_\mathrm{p}, \bar{L}_\mathrm{p}; (1-n'_\mathrm{n}-S_\mathrm{n}), S_\mathrm{n}; (1-n'_\mathrm{p}-S_\mathrm{p}), S_\mathrm{p}) \\
&\qquad \times \prod_{z=\mathrm{n,p}} i^{\bar{L}_z - S_z}(-)^{N_z+L_z+n'_z}\sqrt{(2L_z+1)(2\bar{L}_z+1)(2S_z+1)^3/(2-S_z)} \\
&\qquad \times \langle \bar{L}_z S_z 00|J_z 0\rangle\langle n'_z S_z|n_z S_z\rangle \eta(n_z, S_z, N_z, \bar{L}_z, L_z, S_z, J_z, \gamma_\mathrm{C}). \qquad (2)
\end{aligned}$$

The integral I is given by

$$I(N_\mathrm{n}, \bar{L}_\mathrm{n}; N_\mathrm{p}, \bar{L}_\mathrm{p}; \bar{n}_\mathrm{n}; l_\mathrm{n}; \bar{n}_\mathrm{p}, l_\mathrm{p}) = \int \mathrm{d}r\, \Psi^{(\mathrm{B},J)}_{N_\mathrm{n}\bar{L}_\mathrm{n}}(r)\Psi^{(\mathrm{A})}_{N_\mathrm{p}\bar{L}_\mathrm{p}}(r)\Psi^{(^{14}\mathrm{C})}_{\bar{n}_\mathrm{n}l_\mathrm{n}}(|r-R|)\psi^{(^{14}\mathrm{O})}_{\bar{n}_\mathrm{p}l_\mathrm{p}}(|r-R|). \qquad (3)$$

The radial wave functions $\Psi^{(\mathrm{B},J)}_{N_\mathrm{n}\bar{L}_\mathrm{n}}(r)$ and $\Psi^{(\mathrm{A})}_{N_\mathrm{p}\bar{L}_\mathrm{p}}(r)$ describe the motion of the c.m. of the dinucleon in the residual and target systems, respectively. Similarly $\Psi^{(^{14}\mathrm{C})}_{\bar{n}_\mathrm{n}l_\mathrm{n}}(|r-R|)$ and $\Psi^{(^{14}\mathrm{C})}_{\bar{n}_\mathrm{p}l_\mathrm{p}}(|r-R|)$ are the radial wave functions of the c.m. of the dinucleon in the projectile and ejectile, respectively.

† Therefore, methods such as the one developed in ref. [3]) should be applied in principle.

The nuclear structure information is contained in the factors

$$\eta(n_n, \bar{l}_n, N_n, \bar{L}_n, S_n, J_n, \gamma_C)$$

$$= (-)^{N_n} \sum_{j_{1_n} \geq j_{2_n}} \sqrt{(2j_{1_n}+1)(2j_{2_n}+1)}\, \langle n_n \bar{l}_n,\ N_n \bar{L}_n,\ L_n | n_{1_n}, n_{2_n} l_{2_n},\ L_n \rangle$$

$$\times \begin{Bmatrix} j_{1_n} & l_{1_n} & \frac{1}{2} \\ j_{2_n} & l_{2_n} & \frac{1}{2} \\ J_n & L_n & S_n \end{Bmatrix} \langle \mathrm{B},\ JM | [[C^+_{j1_n} C^+_{j2_n}]^{J_n} / \sqrt{1+\delta_{1,2}} | \gamma_C J_p \rangle]^J_M,$$

$$\eta(n_p, \bar{l}_p, N_p, \bar{L}_p, L_p, S_p, J_p, \gamma_C)$$

$$= \frac{(-)^{N_p}}{\sqrt{2J_p+1}} \sum_{j_{1_p} \geq j_{2_p}} \sqrt{(2j_{1_p}+1)(2j_{2_p}+1)} \langle n_p \bar{l}_p,\ N_p \bar{L}_p\ L_p | n_{1_p} l_{1_p}, n_{2_p} l_{2_p},\ L_p \rangle$$

$$\times \begin{Bmatrix} j_{1_p} & l_{1_p} & \frac{1}{2} \\ j_{2_p} & l_{2_p} & \frac{1}{2} \\ J_p & L_p & S_p \end{Bmatrix} \langle \mathrm{A} | [[C^+_{j1_p} C^+_{j2_p}]^{J_p} / \sqrt{1+\delta_{1,2}}\ | \gamma_C J_p \rangle]^0_0. \tag{5}$$

Here $(n_z, \bar{l}_z)$ are the quantum numbers of the relative motion in the dinucleon z, while $(N_z, \bar{L}_z)$ label the motion of the c.m. L_z, S_z and J_z are the orbital, spin and total angular momentum of the dinucleon, respectively. The j's identify the individual fermion states $(n_{z_i}, l_{z_i}, j_{z_i})$ and (γ_C, J_p) label the states of the large core C. The third factors in (4) and (5) are harmonic oscillator (HO) transformation brackets.

The overlap integrals $\langle n'_z \bar{l}_z | n_z \bar{l}_z \rangle$ over the relative dinucleon variables are calculated using pure harmonic oscillator wave functions. Due to the different size of the large and the small systems, these overlaps do not vanish for $n' \neq n$. For each final state and each kind of particle, the possible relative and c.m. quantum numbers $(n, \bar{l}, N, L)$ are $(n, 0, N, J)$, $(n, 1, N, J+1)$ and $(n, 1, N, J-1)$, where if n is given, then N is fixed through conservation of energy considerations. The large number† of integrals (3) is considerably reduced if we enforce an additional assumption to those introduced in subsect. 2.1:

(e) We ignore the difference in size in the calculation of the overlap of the wave

† For a reaction in the Pb region the maximum value of n is 5–6; thus there are about 400 integrals (3) to be performed for each final state. Using (6) this number is reduced to less than 16.

functions depending on the relative coordinates:

$$\langle n'_z l'_z | n'_z l'_z \rangle = \delta_{n_z n'_z}. \tag{6}$$

In this case the possible† values of (n, l, N, L) are $(0, 0, N, J)$, $(1, 0, N-1, J)$, $(0, 1, N-1, J+1)$ and $(0, 1, N-1, J-1)$, due to the properties of the $(p_{\frac{1}{2}})^2$ configuration in the light systems (see appendix A).

2.3. HEISENBERG PROCESSES

Under similar application of assumptions (a)–(d) one obtains the form factors corresponding to Heisenberg process [see eqs. (A.13)–(A.18)]:

$$\begin{aligned}
&\langle b \equiv {}^{14}\mathrm{O(g.s.)};\ \mathrm{B}(JM)|V(\boldsymbol{r}_t - \boldsymbol{r}_T)\boldsymbol{\tau}_t \cdot \boldsymbol{\tau}_T|\mathrm{A(g.s.)};\ \mathrm{a} \equiv {}^{14}\mathrm{C(g.s.)}\rangle \\
&\quad = V_0^{\mathrm{H}} \frac{i^J}{4\pi^{\frac{1}{2}}\sqrt{2J+1}} Y^*_{JM}(\Omega_R) \\
&\qquad \times \sum_{\substack{n_t S_t N_n \bar{L}_n \\ N_p \bar{L}_p}} I(N_n, \bar{L}_n; N_p, \bar{L}_p; (1-n_t-S_t), S_t; (1-n_t-S_t), S_t) \\
&\qquad \times \sqrt{\frac{(2S_t+1)}{(2-S_t)}} \begin{Bmatrix} 1 & 1 & S_t \\ \frac{1}{2} & \frac{1}{2} & \frac{1}{2} \end{Bmatrix}^2 i^{\bar{L}_n + \bar{L}_p} \langle \bar{L}_n \bar{L}_p 00 | J0 \rangle \\
&\qquad \times \sum_{\substack{L_n L_p J_n J_p \\ n_T S_T l_T \gamma_C}} (-)^{J_p + \bar{L}_n + S_T + l_T} (2S_T+1) \begin{Bmatrix} J_n & S_T & L_n \\ L_p & J & J_p \end{Bmatrix} \begin{Bmatrix} \bar{L}_n & l_T & L_n \\ L_p & J & \bar{L}_p \end{Bmatrix} \\
&\qquad \times \prod_{z=n,p} (2L_z+1)\sqrt{(2J_z+1)(2\bar{L}_z+1)}\,\eta(n_T, l_T, N_z, \bar{L}_z, L_z, S_T, J_z, \gamma_C),
\end{aligned} \tag{7}$$

where the operator τ_t transforms a dineutron into a diproton in the light system and τ_T does the opposite in the heavy system. The integral I is given by eq. (3). In the Heisenberg case, there is no approximation analogous to assumption (e), since each dinucleon stays in the same system.

3. Numerical results

3.1. INGREDIENTS AND FEATURES OF THE DWBA

Most of the present study is based on the comparison of angle-integrated cross

† See footnote on previous page.

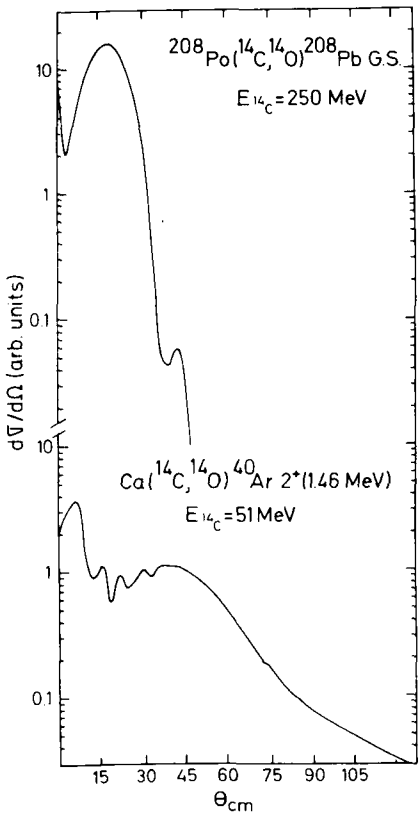

Fig. 2. Typical angular distributions obtained with the Heisenberg form factors and the optical model parameters of table 1. The set II is used for the $^{208}Po(^{14}C, ^{14}O)^{208}Pb$ reaction.

sections. Typical angular distributions are shown in fig. 2 for the reactions $^{208}Po(^{14}C, ^{14}O)^{208}Pb$ and $^{40}Ca(^{14}C, ^{14}O)^{40}Ar$. They were calculated with the code DWUCK4 [4]. Some important features of the results can be understood by analyzing the ingredients in the reaction amplitude T (eq. (1)), namely the distorted wave functions χ and the form factor $\langle bB|V|aA\rangle$.

The functions are obtained by solving an optical model hamiltonian with the parameters given in table 1. For the reaction $^{208}Po(^{14}C, ^{14}O)^{208}Pb$ two different sets are used with results disagreeing by only a few percents. The extended nature of the projectile (ejectile) is taken into account by using effective radii for the target (residual) nucleus. Depending on the projectile energy, up to 150 partial waves are considered.

These reactions imply a sizable angular momentum mismatch (especially for heavy target nuclei) mainly due to the difference in the Coulomb barriers V_{CB} between the incoming and outgoing channels. Table 2 lists the difference Δl_{gr} in the grazing angular momentum for different incident energies and target nuclei. Use

TABLE 1

Optical model and bound-state parameters

Reaction	V (MeV)	r_{0V} (fm)	a_{0V} (fm)	W (MeV)	r_{0W} (fm)	a_{0W} (fm)	r_{0C} (fm)	Ref.
$^{208}Po + ^{14}C$, set I	40	1.31 [a])	0.45	15	1.31 [a])	0.45	1.3 [a])	[5])
$^{208}Po + ^{14}O$, set II	51.09	[a,b])	[c])	51.46	[a,b])	[d])	1.3 [a])	[6])
$^{40}Ca + ^{14}C$	35.2	1.4 [a])	0.493	61.4	1.2 [a])	0.3	1.4 [a])	[7])
$^{40}Ar + ^{14}O$								
$^{206}Pb + 2$ nucleons	[e])	1.28	0.76				1.3	[5])
$^{38}Ar + 2$ nucleons	[e])	1.20	0.65				1.3	[7])
$^{12}C + 2$ nucleons	[f])	1.25	0.65				1.3	[5])

[a]) $R_x = r_{0x}(A_1^{1/3} + A_2^{1/3})$ ($x = V$ or W).
[b]) $r_{0V} = r_{0W} = 1.653 - 0.0471E_{lab} + 0.0000109E_{lab}^2$.
[c]) $a_{0V} = 0.651 - 0.01546E_{lab} - 0.0000425E_{lab}^2$.
[d]) $a_{0W} = 0.629 + 0.01416E_{lab} - 0.0000369E_{lab}^2$.
[e]) Adjusted to give the binding energies, see eqs. (13).
[f]) Adjusted to give the binding energies, see eqs. (12).

has been made of the expression [8])

$$l_{gr} = 0.22\, R_C \sqrt{\mu(E_{c.m.} - V_{CB})}, \tag{8}$$

where μ is the reduced mass, $E_{c.m.}$ the energy in the c.m. system and

$$V_{CB} = e^2 Z_1 Z_2 / R_C, \tag{9a}$$

$$R_C = 0.5 + 1.36(A_1^{\frac{1}{3}} + A_2^{\frac{1}{3}}). \tag{9b}$$

In order to indicate the extent to which the angular momentum mismatch influences the cross-section magnitudes, calculations were performed assuming the same form factor, incident and outgoing energies but different transferred angular momenta J. The sample case corresponds to the reaction $^{208}Po(^{14}C, ^{14}O)^{208}Pb$ (fig. 3). We note that the curve shows a maximum for values of the transferred angular momentum $J \approx 7$ which is the Δl_{gr} predicted for this case (table 2).

TABLE 2

Entrance-exit differences in the grazing angular momentum

Reaction	$^{40}Ca(^{14}C, ^{14}O)$		$^{48}Ti(^{14}C, ^{14}O)$			$^{56}Fe(^{16}O, ^{16}C)$		$^{146}Sn(^{16}O, ^{16}C)$				$^{208}Po(^{14}C, ^{14}O)$		
E_{lab} (MeV)	51	120	50	100	150	150	180	80	100	150	180	100	150	200
$\Delta l_{gr}(\hbar)$	8	3	15	6	5	8	7	16	9	5	4	19	11	7

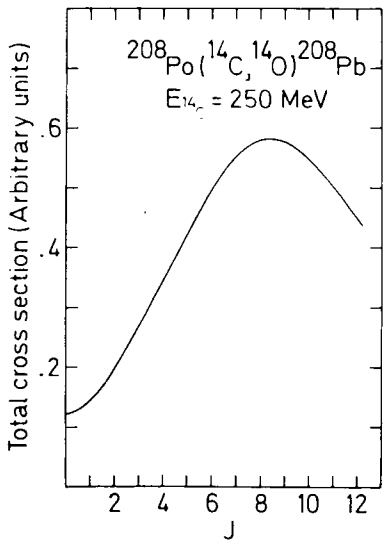

Fig. 3. The angle-integrated cross section as a function of the transferred angular momentum.

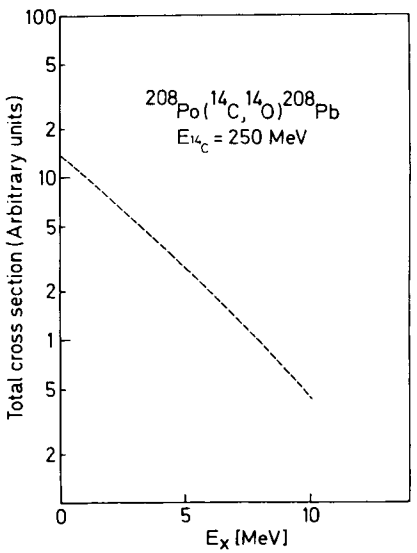

Fig. 4. The angle-integrated cross section as a function of the excitation energy. The same form factor as for the case of fig. 3 has been used.

Similarly fig. 4 shows Q-effects in the total cross section. The consequences of the interplay of this effect and the angular momentum mismatch on the population of actual states are discussed in subsect. 3.2.

The form factors $\langle bB|V|aA\rangle$ are calculated using the formulae (2) or (7). They contain the integrals (3) constructed through a convolution between a product of the c.m. of a diproton and a dineutron wave function $\Psi_{N\bar{L}}(r)$ in target and residual nucleus, respectively, and the corresponding product of the dinucleon wave functions $\Psi_{\bar{n}l}(|r-R|)$ in the projectile and ejectile.

Each product, corresponding to the light and heavy systems, respectively, has an exponential-like asymptotic behavior. The asymptotic values of the form factors (2) or (7) are then dominated by the exponential decay of that product which decreases more slowly. In the cases listed in table 2 this is always the product of wave functions corresponding to the light system. Thus, all form factors decay asymptotically with similar slopes:

$$\exp\left(-\kappa^{(^{14}C)}R-\kappa^{(^{14}O)}R-\eta^{(^{14}O)}l\eta 2\kappa^{(^{14}O)}R\right), \tag{10}$$

where

$$\kappa^{(^{14}C)}\approx 1.04\ \text{fm}^{-1}, \qquad \kappa^{(^{14}O)}\approx 0.73\ \text{fm}^{-1} \tag{11}$$

and $\eta^{(^{14}O)}$ is the Sommerfeld parameter for a diproton in the ^{12}C electric field.

For the actual calculation of the integrals (3), first the four wave functions $\Psi_{\bar{n}_n l_n}$, $\Psi_{\bar{n}_p l_p}$, $\Psi_{N_n\bar{L}_n}$ and $\Psi_{N_p\bar{L}_p}$ are obtained by solving Saxon-Woods potentials that yield empirical dinucleon separation energies. For the $A = 14$ projectile (ejectile) system, it corresponds to the energy needed to separate a dineutron (diproton) from the $^{14}C(^{14}O)$ nucleus to obtain a ^{12}C ground-state core:

$$E(\bar{n}_n l_n) = \text{BE}(^{14}C)-\text{BE}(^{12}C) = 13.12\ \text{MeV}, \tag{12a}$$

$$E(\bar{n}_p l_p) = \text{BE}(^{14}O)-\text{BE}(^{12}C) = 6.57\ \text{MeV}. \tag{12b}$$

For the heavier target (residual) system the functions $\Psi_{N\bar{L}}$ entering in the integrals (3) depend on the state $|\gamma_C J_C\rangle$ of the core C that contributes for the final state $|B, J\rangle$ under consideration [see eqs. (2) and (7)],

$$E(N_n\bar{L}_n) = \text{BE}(B, J)-\text{BE}(\gamma_C J_C), \tag{13a}$$

$$E(N_p\bar{L}_p) = \text{BE}(A, \text{g.s.})-\text{BE}(\gamma_C J_C). \tag{13b}$$

Once the functions Ψ have been obtained for values of r ranging from 0.1 fm to 22.0 fm in steps of 0.1 fm, the convolutions of eq. (3) are performed for given values of the distance R between the cores C and c. Then, the form factors $\langle bB|V|aA\rangle$ as

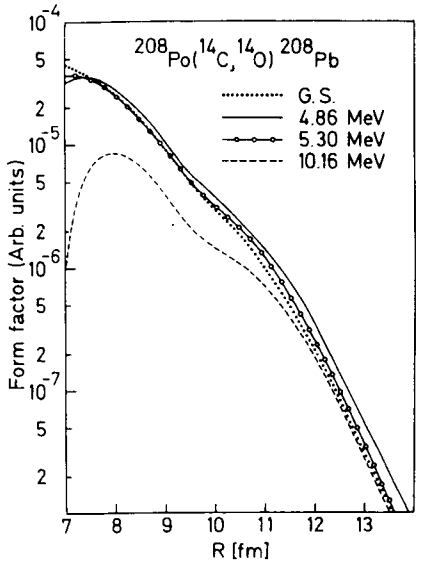

Fig. 5. Heisenberg form factors corresponding to the population of four 0^+ states in ^{208}Pb. The populated states are the ground state, 4.86 MeV (neutron pairing vibration), 5.30 MeV (proton pairing vibration) and 10.16 MeV ("alpha-vibration").

a function of R results from the addition of integrals (3) multiplied by nuclear structure (η) and angular momentum coefficients [formulae (2) or (7)]. Since in general this implies the summation of several hundred terms for each final state and distance R, the calculation is only performed for values starting at $R_{min} = 7$ fm and going up to 15 fm in steps of 0.5 fm. Finally the form factors are interpolated within the said interval and extrapolated to $R_{max} = 18$ fm in steps of 0.1 fm and in this manner are read in to the code DWUCK4.

Examples of form factors are given in fig. 5 for the population of different 0^+ states in ^{208}Pb. As discussed before, all of them present the same asymptotic behavior. The useful region of integration starts approximately at the channel radius, which in these examples is 9.75 fm. At this distance the asymptotic regime is far from valid. The upper end of the useful region is partly determined by the exponential decay, and partly by the behavior of the distorted waves. Due to the angular momentum mismatch, for instance, the first maximum of the grazing partial wave in the incoming channel ($l_{gr} = 124$) is at ≈ 11.8 fm, while for the same partial wave, the maximum is at ≈ 12.6 fm in the exit channel for the g.s. transition. Table 3 lists values of g.s. cross sections as a function of a lower cut-off in the form factors. From this table one concludes that the relevant region of integration lies between 9.5 fm and 13 fm thus justifying the choice of $R_{min} = 7$ fm.

TABLE 3

Effect of the lower cut-off radius

R_{min} (fm)	7.0	7.5	8.0	8.5	9.0	9.5	10.0	10.5	11.0	11.5	12.0	12.5	13.0	13.5	14.0	14.5
σ_{tot}	1961	1961	1961	1962	1966	1981	2035	2469	2894	1894	670	171	51	3	0.1	0.01

Angle-integrated cross section (arbitrary units) as a function of the lower cut-off R_{min} of the form factor for the reaction $^{208}Po(^{14}C, ^{14}O)^{208}Pb$ (g.s.). The form factor is given in fig. 5 and the incident energy is 250 MeV.

3.2. MICROSCOPIC FEATURES

An approximate but physically simple estimate of the relative cross sections in the reaction $^{208}Po(^{14}C, ^{14}O)^{208}Pb$ can be obtained using experimental results of two-neutron transfer reactions (p, t) and (t, p). Both of these two reactions collectively populate the g.s., particle-hole states and two-particle – two-holes states (pairing vibrations) in ^{208}Pb. This simple estimate suggests the possibility of relatively strong cross sections populating states up to four-particles–four-holes. Results calculated in the framework of the above approximation have been presented in ref. [9]) and are summarized in the fourth column of table 4. The main

TABLE 4

Cross sections for $^{208}Po(^{14}C, ^{14}O)^{208}Pb$

E_x (MeV)	J^π	Configuration	Estimate of ref. [9])	Wigner processes	Heisenberg processes
0 [a])	0^+	g.s.	1	1	1
2.61 [a])	3^-	(ph, 3)	0.66	0.29	0.16
3.20 [a])	5^-	(ph, 5)	1.5	1.1	0.03
4.86 [a])	0^+	(r, n, 0)(a, n, 0)	0.44	2.4	0.60
5.22	6^+	$(ph, 3)^2$	0.01	0.002	0.00001
5.30	0^+	(r, p, 0)(a, p, 0)	2.3	0.15	0.32
5.65 [b])	2^+	(r, n, 0)(a, n, 2)	1.1	0.13	0.04
5.81	8^+	(ph, 3)(ph, 5)	0.05	0.005	0.0002
6.37	2^+	(r, p, 2)(a, p, 0)	1.8	0.13	0.01
6.40	10^+	$(ph, 5)^2$	0.04	0.004	0.003
10.16	0^+	(r, n, 0)(a, n, 0)(r, p, 0)(a, p, 0)	1.0	0.22	0.03

Estimated angle-integrated cross section (relative to g.s.) for the reaction $^{208}Po(^{14}C, ^{14}O)^{208}Pb$ at the incident energy of 250 MeV. In the case of states with two or four phonons, the listed energy is the sum of the energies corresponding to the single-phonon states. The third column displays the phonon configurations of each final state. The fourth column displays the rough estimate obtained in ref. [9]) through two-neutron stripping and pick-up experiments with light ions.

[a]) State experimentally known.

[b]) State experimenta.ly known to be split at 5.55 MeV and 5.80 MeV.

drawbacks of this calculation are: (i) the use of two neutron-transfer results in place of the two-proton ones; (ii) the transfer of the two dinucleons only in $S = 0$ states (as they are in ^3H or ^3He); (iii) the fact that effects due to angular momentum mismatch and Q-effects (figs. 3 and 4) are ignored.

In the present paper we attempt to make a better estimate of these relative cross sections avoiding the previous shortcomings.

From the microscopic point of view, the fact that the pair of neutrons in the triton is mainly in a singlet state and that the nucleons are at relatively short distances from each other, make the (t, p) reaction a good probe of the correlation between pairs of neutrons in the final system. Since that reaction strongly populates states in which the neutrons are closer to each other, for these states all amplitudes in the construction of the form factors corresponding to different configurations are in phase. However in the present case, the singlet and triplet states have similar probability in the $[(p_{\frac{1}{2}})^2]$ configuration of the dinucleon in the light systems. The above-mentioned coherence is no longer present in the triplet contributions. However, and although systematically somewhat smaller, these are generally of the same order of magnitude as the singlet contributions.

The influence of these and other facts in the calculation of the form factors will be now discussed in detail, beginning with the 0^+ states (g.s., two-phonon pairing vibrations at 4.86 MeV and 5.30 MeV and the four-phonon 10.16 MeV state). To this end in table 5 we label the structure factors [eqs. (4) and (5)] by the type of nucleons (z = n or p) and by the number of pairing addition or removal phonons ($n_{p.v.}$ = number of phonons, see appendix B). In Heisenberg processes both kind of particles are either in the singlet or in the triplet state. On the contrary, in Wigner processes, there can be interference effects due to neutron-singlet, proton-triplet contributions (and vice versa). In the population of the g.s. (factors $\eta_{n,0}$ and $\eta_{p,0}$ in table 5), there is a cancellation due to this interference terms. In the population of the neutron vibrational state at 4.86 MeV, the neutron factors $\eta_{n,2}$ and the proton factors $\eta_{p,0}$ are used. In this case, the neutron-triplet proton-singlet contribution has the same phase as the singlet-singlet and triplet-triplet terms. Hence, we understand the larger population of the 4.86 MeV 0^+ relative to the g.s. population in Wigner processes, and the fact that this enhancement is not present for Heisenberg processes.

The population of the predicted proton state at 5.30 MeV has similar features to the population of the g.s. In this case, the neutron factors $\eta_{n,0}$ and the proton factors $\eta_{p,2}$ are used. For Wigner processes, there is a significant neutron-singlet proton-triplet contribution which tends to cancel the singlet-singlet and triplet-triplet contributions.

In the population of the 10.16 MeV 0^+ state, the factors $\eta_{n,2}$ and $\eta_{p,2}$ are used. In Wigner processes the crossed contributions (neutron-triplet proton-singlet and neutron-singlet proton-triplet) tend to cancel each other; this is also true for the singlet-singlet and triplet-triplet contributions in both Heisenberg and Wigner processes.

TABLE 5

Contributions to the structure factors (0^+ states)

$n_{p.v.}$				0						2					
z			n				p				n			p	
N		5	4	4		5	4	4		6	5	5		4	3	1
n		0	1	0		0	1	0		0	1	0		0	1	0
s		0	0	1		0	0	1		0	0	1		0	0	1
	$(0h_{9/2})^2$	−1	−3	1	$(0h_{9/2})^2$	4	15	−3	$(1g_{9/2})^2$	11	24	6	$(0g_{7/2})^2$	−1	−5	1
	$(1f_{7/2})^2$	−4	−6	−2	$(1f_{7/2})^2$	8	11	3	$(0i_{11/2})^2$	1	5	−1	$(1d_{5/2})^2$	−8	−6	−3
	$(0i_{13/2})^2$	−1	−6	−1	$(0i_{13/2})^2$	1	6	1	$(1j_{15/2})^2$	1	4	1	$(0h_{11/2})^2$	−4	−13	−2
	$(2p_{3/2})^2$	−9	1	−1	$(2p_{3/2})^2$	3	4	−2	$(2d_{5/2})^2$	5	2	1	$(1d_{3/2})^2$	−14	−11	7
	$(1f_{5/2})^2$	−8	−12	5	$(1f_{5/2})^2$	4	0	1	$(3s_{1/2})^2$	2	−1	0	$(2s_{1/2})^2$	−20	8	0
	$(2p_{1/2})^2$	−18	1	5	$(2p_{1/2})^2$	2	0	−1	$(1g_{7/2})^2$	2	4	−1				
									$(2d_{3/2})^2$	2	1	−1				
$\eta(z, n_{p.v.})$		−41	−24	7		22	36	−1		24	38	5		−48	−27	3

The different contributions to the factors $\eta(n, s, N, 0, s, s, s, \gamma_c)$ [eqs. (4) and (5)] in the population of 0^+ states of ^{208}Pb (in units of 10^{-2}); z = n or p for neutrons and protons, respectively, and $n_{p.v}$ = number of pairing phonons.

However, it is clear that arguments taken from structure considerations alone cannot explain the total cross sections. For instance, another effect which influences the relative population of neutron and proton pairing excitations is the fact that the neutron pair is stripped to the shell above, into states with less binding energy and possible larger c.m. radial quantum numbers N. On the contrary, the protons are captured from states with more binding than in the g.s., belonging to the shell below. Therefore, the overlap with the corresponding dinucleon in the projectile becomes more favourable in the first case than in the second.

The Q-effects are also important. Fig. 4 indicates that we may expect a factor of ≈ 30 decreasing the population of the 10.16 MeV state relatively to the g.s.

The two 2^+ states listed in tables 4 belong also to the pairing family. They are predicted to be populated with small but significant probabilities. The neutron double-phonon state predicted at 5.66 MeV is known [10,11]) to be split into two states at 5.59 MeV and 5.80 MeV, respectively.

The population of the particle-hole states in ^{208}Pb is made via two paths. In the first one, the neutron structure factors are obtained through matrix elements involving both a pairing removal and a particle-hole phonon amplitude λ [see eq. (B.8)], while the proton factors are as in $\eta_{p,0}$ of table 5. In the second path, the neutron factors are the $\eta_{n,0}$ of table 5, while the proton ones involve the proton addition and the particle-hole proton-phonon amplitudes as in (B.9). The important contributions to the neutron factors in the first path and to the proton factors in the second path are given in tables 6 and 7 for the population of the 2.61 MeV 3^- and 3.20 MeV 5^- states, respectively.

In both tables the proton factors are considerable smaller, reflecting less participation of the protons than of the neutrons in the particle-hole states. Therefore the first path yields the dominant contribution.

In the population of the 3^- state via the first path, the requirement of a large component in the neutron removal phonon favours the $(p_{\frac{1}{2}})^{-2}$ configuration, and thus the two particle-hole contributions $(g_{\frac{7}{2}}p_{\frac{1}{2}}^{-1})^{3-}$ and $(d_{\frac{5}{2}}p_{\frac{1}{2}}^{-1})^{3-}$. The first one should be larger since the reduced single-particle matrix element $\langle g_{\frac{7}{2}}||Y_3||p_{\frac{1}{2}}\rangle$ does not involve a spin-flip, while $\langle d_{\frac{5}{2}}||Y_3||p_{\frac{1}{2}}\rangle$ does. Accordingly, there is a dominating neutron contribution in table 6. Concerning the comparison between Wigner and Heisenberg processes, one sees that there are two large, mutually cancelling, triplet neutron factors (table 6) and a small triplet proton factor $\eta_{p,0}$ (table 5). Therefore, the singlet-singlet contributions are expected to dominate in both Wigner and Heisenberg. Thus, the relative population of the 3^- state is similar in both processes.

There is a significant difference between the Wigner and the Heisenberg cross sections to the 5^- state. In this case it is difficult to produce a qualitative explanation since both are the result of many cancellations: the two singlet contributions have opposite signs, as well as the two largest triplet contributions (table 7).

TABLE 6

Contributions to the structure factors (3^- state)

	$\bar{L}$	3	3	2	2	4	4
z	L	3	3	3	2	3	4
	n	0	1	0	0	0	0
	s	0	0	1	1	1	1
neutrons	N	4	3	4	4	3	3
	$d_{5/2}\,p_{1/2}$	− 3	1	− 1	1	0	0
	$g_{7/2}\,p_{1/2}$	21	16	−13	0	−10	−11
	$s_{1/2}\,f_{5/2}$	− 1	0	0	0	1	0
	$g_{7/2}\,f_{5/2}$	− 1	− 1	0	1	0	1
	$d_{3/2}\,f_{5/2}$	1	0	0	0	0	−1
	$\eta(nsN\bar{L}Ls3, \text{g.s.})$	17	16	−14	2	− 9	−11
protons	N	3	2	3	3	2	2
	$f_{5/2}s_{1/2}$	− 2	0	1	0	1	0
	$h_{9/2}\,d_{3/2}$	0	1	0	0	0	0
	$f_{5/2}\,d_{3/2}$	− 1	− 1	0	1	0	2
	$p_{3/2}\,d_{3/2}$	− 3	1	0	1	1	0
	$\eta(nsN\bar{L}Ls3, 3^-)$	− 6	1	1	2	2	2

Contributions to the structure factors η [eqs. (4) and (5)] for the population of the 2.61 MeV, 3^- state in ^{208}Pb. The values are given in units of 10^{-3}, and only contributors with at least one contribution larger than 10^{-3} are listed.

The predicted population of two- (particle-hole) phonon states is always weak. From the point of view of structure considerations, this can be explained because the proton factors of tables 6 and 7 enter in all possible paths and are always small [see also eqs. (B.13) and (B.15)]. From the point of view of the reaction mechanism, the Q-effects decrease the population of states at higher energies (fig. 4) thus cancelling the possible effect of the angular momentum mismatch, which would favor the highest angular momentum state of the multiplet (fig. 3). Therefore, the long search for the double octupole phonon state is not likely to be settled through pair-exchange reactions.

3.3. THE VALIDITY OF ASSUMPTION (e)

The results of a calculation removing assumption (e) (i.e. taking into account the effects of the difference in the size of the light and heavy ions in the calculation of the overlap in the relative dinucleon motion) are presented in table 8 for 0^+ states.

TABLE 7

Contributions to the structure factors (5^- state)

	$\bar{L}$	5	5	4	4	6	6
z	L	5	5	5	4	5	6
	n	0	1	0	0	0	0
	s	0	0	1	1	1	1
neutrons	N	3	2	3	3	2	2
	$g_{9/2}p_{1/2}$	−6	0	−3	2	−2	0
	$i_{11/2}p_{1/2}$	3	6	−3	0	−3	−2
	$i_{11/2}f_{5/2}$	−1	−2	0	0	0	1
	$d_{5/2}f_{5/2}$	−5	1	0	1	2	0
	$g_{7/2}f_{5/2}$	2	2	0	−1	0	−4
	$g_{7/2}p_{3/2}$	−4	0	0	0	1	0
	η	−11	7	−6	2	−2	−5
protons	N	2	1	2	2	1	1
	$h_{9/2}g_{7/2}$	0	1	0	0	0	−1
	$h_{9/2}d_{5/2}$	−1	−1	1	0	1	−1
	$h_{9/2}d_{3/2}$	−1	−2	0	0	0	2
	$h_{9/2}s_{1/2}$	2	2	−2	0	−2	0
	$f_{7/2}f_{5/2}$	1	0	0	1	0	0
	$f_{7/2}d_{3/2}$	3	−1	1	−1	0	0
	$f_{5/2}d_{5/2}$	2	0	0	0	0	0
	η	7	0	0	0	−2	0

Contributions to the structure factors η [eqs. (4) and (5)] for the population of the 3.20 MeV, 5^- state in ^{208}Pb. The values are given in units of 10^{-3}, and only contributors with at least one contribution larger than 10^{-3} are listed.

One notices that the relative population of the neutron pairing vibrational state is reduced.

In order to understand this effect, the factors $\langle n's|ns\rangle\eta(n, s, N, s, s, 0, \text{g.s.})$ are listed for the g.s. neutron transitions in the $^{208}Po(^{14}C, ^{14}O)^{208}Pb$ reaction in table 9. For each column, assumption (e) would yield the single contribution that is displayed between parenthesis in the line labelled by the corresponding value of N. Although assumption (e) is well supported by the results listed in columns one and three (in the sense that there is a predominant contribution) the approximation looks less appropriate in the case of the second column.

Each of the 17 neutron contributions appearing in table 9 must be multiplied by the corresponding proton contributions. Subsequently these products are weighted

TABLE 8

Effect on the cross sections of removing assumption (e)

E_x (MeV)	Configuration	With ass.(e)	Without ass.(e)
0	g.s.	1	1
4.86	$[(r, n, 0)(a, n, 0)]^0$	2.4	1.4
5.30	$[(r, p, 0)(a, p, 0)]^0$	0.16	0.23

Results of relative population of 0^+ states in ^{208}Pb including assumption (e) (column 3) and removing it (column 4). The same incident energy and optical model parameters as for table 4 are used.

by geometrical factors and integrals (3) and then finally added. The validity of assumption (e) is further supported by the fact that the integrals involving larger values of N_n, N_p have more weight than the ones with small c.m. radial quantum number. Should the final sum be incoherent, we may conclude that assumption (e) is acceptable. However, since the sum is coherent, we must note that all the contributions corresponding to zero spin have the same sign, but for the $n' = 1$, $N = 5$ case (see column one and two of table 9). On the contrary, the spin-one contributions show more fluctuations in sign (column three). From our analysis of subsect. 3.2 it appeared as a cancellation between $S = 0$ and $S = 1$ contributions in the g.s. transition, and as an enhancement in the case of the neutron pairing vibrational state at 4.86 MeV. Therefore, we understand why removal of

TABLE 9

Effect on the neutron structure factor of removing assumption (e)

N	$(n's) = (0,0)$	$(1,0)$	$(0,1)$
5	−35(−41)	18	
4	−11	−12(−24)	6(7)
3	− 6	−15	−1
2	− 2	−11	0
1	− 1	− 6	0
0	− 1	− 6	1
	−56	−32	6

The value of the products $\langle n's|ns\rangle\ \eta(n, s, N, s, s, s, 0, \text{g.s.})$ for the ground-state transition in the $^{208}Po(^{14}C, ^{14}O)^{208}Pb$ reaction (in units of 10^{-2}). n is fixed by the condition on the HO transformation brackets $n = 5-N$. Although the sums of each column listed in the last line have no direct physical meaning (see text) they give an indication of a relative increase in the contributions with zero spin to those with spin one. The numbers in parentheses are the ones obtained using eq. (6) and the last line of table 5.

assumption (e) goes in the direction of reducing the relative population of the neutron pairing vibration (states at 4.86 MeV and 10.16 MeV).

The predicted reduction may be interpreted as follows: the short-range residual interaction of the pairing type tends to bring the particles closer to each other and thus to produce a larger overlap of the relative motion in the heavy system and in the light system. This effect appears usually in the spin-zero contributions, where there is no spatial Pauli repulsion; thus, the sensibility of the results to the relative weight of spin-0 and spin-1 contributions.

3.4. POINT APPROXIMATION

In the Heisenberg type of processes, a further approximation can be made: one may assume that neither the projectile nor the ejectile have structure. Therefore, the light system is a point particle with coordinate $\boldsymbol{R}$ and isospin one. The operator τ_t transforms the ^{14}C projectile into the ^{14}O ejectile. In this case, the form factor becomes identical to the one appearing in the single-charge-exchange processes with very light ions. From eq. (A.18) we obtain

$$\begin{aligned}
&\langle {}^{14}\mathrm{O(g.s.)};\ \mathrm{B}(JM)|V(|\boldsymbol{R}-\boldsymbol{r}_\mathrm{T}|)\boldsymbol{\tau}_t\cdot\boldsymbol{\tau}_\mathrm{T}|\mathrm{A(g.s.)};\ {}^{14}\mathrm{C(g.s.)}\rangle \\
&\quad=(-)^{J+M}\sum_{\substack{n_\mathrm{C}J_\mathrm{p}J_\mathrm{p}n_\mathrm{T}S_\mathrm{T}l_\mathrm{T}\\ N_\mathrm{p}\bar{L}_\mathrm{p}L_\mathrm{p}N_\mathrm{n}\bar{L}_\mathrm{n}L_\mathrm{n}}}(-)^{J_\mathrm{p}+\bar{L}_\mathrm{p}+l_\mathrm{T}+S_\mathrm{T}}(2S_\mathrm{T}+1) \\
&\qquad\times\begin{Bmatrix} J_\mathrm{n} & S_\mathrm{T} & L_\mathrm{n}\\ L_\mathrm{p} & J & \bar{L}_\mathrm{p}\end{Bmatrix}\begin{Bmatrix}\bar{L}_\mathrm{n} & l_\mathrm{T} & L_\mathrm{n}\\ L_\mathrm{p} & J & \bar{L}_\mathrm{p}\end{Bmatrix} \\
&\qquad\times\sum_{z=\mathrm{n,p}}(2L_z+1)\eta(n_\mathrm{T},\ l_\mathrm{T},\ N_z,\ \bar{L}_z,\ L_z,\ S_\mathrm{T},\ J_z,\ n_\mathrm{C}) \\
&\qquad\times\int \mathrm{d}\boldsymbol{r}_\mathrm{T}V(|\boldsymbol{R}-\boldsymbol{r}_t|)[\Phi^{\mathrm{B}(L)}_{N_\mathrm{n}\bar{L}_\mathrm{n}}(\boldsymbol{r}_\mathrm{T})\Phi^{\mathrm{A}}_{N_\mathrm{p}L_\mathrm{p}}(\boldsymbol{r}_\mathrm{T})]^J_M. \qquad (14)
\end{aligned}$$

Upon application of the Buttle-Goldfarb approximation the integral in the previous equation reduces to a one-dimensional integral:

$$\begin{aligned}
&\frac{i^{\bar{L}_\mathrm{n}+\bar{L}_\mathrm{p}-J}}{2\pi^{\frac{1}{2}}\sqrt{2J+1}}\langle\bar{L}_\mathrm{n}\bar{L}_\mathrm{p}00|J0\rangle\sqrt{(2\bar{L}_\mathrm{n}+1)(2\bar{L}_\mathrm{p}+1)}\,Y^*_{JM}(\Omega_R) \\
&\qquad\times\int \mathrm{d}r_\mathrm{T}V(|R-r_\mathrm{T}|)\Psi^{\mathrm{B}(J)}_{N_\mathrm{n}\bar{L}_\mathrm{n}}(r_\mathrm{T})\Psi^{(\mathrm{A})}_{N_\mathrm{p}L_\mathrm{p}}(r_\mathrm{T}). \qquad (15)
\end{aligned}$$

There are at least two objections associated with the point approximation, namely:

(i) According to the discussion on the macroscopic aspects of the reaction, the form factor decays asymptotically as the product of the wave functions of the c.m. of the dinucleon in the projectile (ejectile). However, the form factor in the point approximation decays as the product of the corresponding wave functions in the target (residual) system, which is faster. The ratio between the "point" and the Heisenberg decay parameters κ entering in the asymptotic exponential $e^{-\chi R}$ is about 1.4 [compare with eqs. (10) and (11)].

(ii) The relevant region of integration in the DWBA has a lower cut-off of about 9.5 fm (subsect. 3.1) corresponding to the sum of the target (R_T) and projectile radius (R_t). At this distance, the exponential decay has induced a decrease $e^{-\kappa R}$ from the value of the form factor at the target radius R_T which is of three orders of magnitude (R_t = 2.9 fm). On the contrary, the construction of the form factors by taking into account the (extended) $(p_{\frac{1}{2}})^2$ dinucleon configuration allows for a better overlap between the dinucleons in the heavy and light systems.

In spite of these objections we have carried out the (simpler) calculations with the point approximation. The results are compared with the Heisenberg calculation (from which it derives) in table 10. Although there are some qualitative agreements, there are quantitative differences which may impose caution in the application of the point approximation.

TABLE 10

Effect on the cross sections of the point approximation

E_x (MeV)	J^π	Heisenberg process	Point approximation
0	0^+	1	1
2.61	3^-	0.16	0.59
3.20	5^-	0.03	0.07
4.86	0^+	0.60	3.29
5.22	6^+	0.00001	0.00001
5.30	0^+	0.32	0.23
5.65	2^+	0.04	0.46
5.81	8^+	0.0002	0.005
6.37	2^+	0.01	0.17
6.40	10^+	0.003	0.003

Angle-integrated cross sections (relative to the g.s.) for the reaction $^{208}Po(^{14}C, ^{14}O)^{208}Pb$ calculated with the point approximation (column 4) compared with the Heisenberg prediction (column 3). The calculation is performed for the same incident energy and optical model parameters as for table 4.

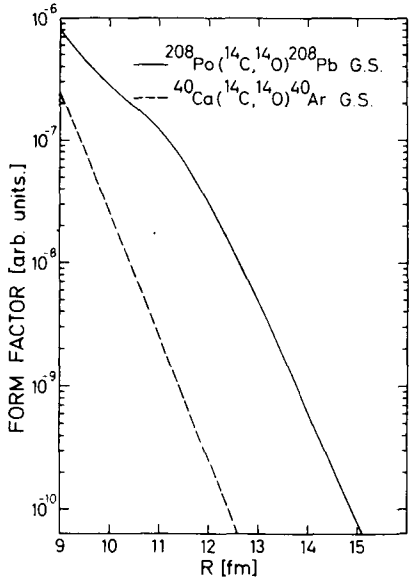

Fig. 6. Form factors (Wigner process) at large radii showing that the asymptotic exponential behavior is independent of the heavier system ($A = 40$ or 208) and is determined by the binding energies of the dinucleons in the $A = 14$ systems.

3.5. THE REACTION $^{40}Ca(^{14}C, ^{14}O)^{40}Ar$

As discussed in the case of the Po target, the asymptotic behavior of the form factor depends only on the binding energies of the dinucleons in the lighter fragments. This is confirmed in fig. 6 where the form factors at large distances are displayed for the g.s. population of both ^{208}Pb and ^{40}Ar systems (Wigner processes).

The pair-exchange reaction on ^{40}C has been performed [2]) at an incoming energy of 51 MeV. At this energy not only there is a sizeable angular momentum mismatch (table 2) but the ^{14}C projectile barely overcomes the Coulomb repulsion. The g.s. and an excited 2^+ state at 1.46 MeV are populated with similar intensities.

The calculations are made assuming a pure dineutron particle configuration $[(f_{\frac{7}{2}})^2]^{0,2}$ and a pure diproton hole configuration $[(p_{\frac{3}{2}})^{-2}]^{0,2}$ in ^{40}Ar. The wave functions are

$$|^{40}\mathrm{Ar(g.s.)}\rangle = \tfrac{1}{2}[C^+_{\frac{7}{2}}C^+_{\frac{7}{2}}]^0[C_{\frac{3}{2}}C_{\frac{3}{2}}]^0|^{40}\mathrm{Ca(g.s.)}\rangle,$$

$$|^{40}\mathrm{Ar}(2^+;\ 1.4\ \mathrm{MeV})\rangle = 0.375\ [C^+_{\frac{7}{2}}C^+_{\frac{7}{2}}]^2[C_{\frac{3}{2}}C_{\frac{3}{2}}]^0|^{40}\mathrm{Ca(g.s.)}\rangle$$
$$-0.250\ [C^+_{\frac{7}{2}}C^+_{\frac{7}{2}}]^0[C_{\frac{3}{2}}C_{\frac{3}{2}}]^2|^{40}\mathrm{Ca(g.s.)}\rangle. \qquad (16)$$

The relative amplitudes of the two components in the 2^+ state represent a

TABLE 11

Contributions to the structure factors in ^{40}Ar

Z	Neutrons					Protons		
N	3	2	2			2	2	2
$\bar{L}$	0	0	1			0	0	1
L	0	0	1			0	0	1
n	0	1	0			0	1	0
s	0	0	1			0	0	1
η	0.17	−0.45	−0.10			0.26	−0.47	0.18
N	2	1	2	1	1	0	1	1
$\bar{L}$	2	2	1	3	2	2	1	3
L	2	2	1	3	2	2	1	3
n	0	1	0	0	0	1	0	0
s	0	0	1	1	0	0	1	1
η	0.34	−0.08	0.07	−0.02	−0.03	0.05	0.03	0.06

Contributions to the structure factors η [eqs. (4) and (5)] for the population of the ground and 1.46 MeV states in ^{40}Ar.

reasonable but certainly not proved value [see ref. [12])]. The structure factors are listed in table 11. The chosen pure configurations exclude the build up of any collectivity in the $S = 0$ channels (as was the case in Pb). Consistently the final results are very sensitive to the selected configurations and to the type of process (Wigner or Heisenberg) that has been assumed (see table 12).

Two-step processes. For the reaction on ^{40}Ca a rough estimate of the relative contribution of two-step mechanisms has been made. Two different paths have been chosen, namely $^{40}Ca(^{14}C, ^{16}O)^{38}Ar(^{16}O, ^{14}O)^{40}Ar$ and $^{40}Ca(^{14}C, ^{12}C)^{42}Ca(^{12}C, ^{14}O)^{40}Ar$. These two nucleons sequential transfers are supposed to be the largest higher-order processes contributing to the $^{40}Ca(^{14}C, ^{14}O)^{40}Ar$ reaction. The strengths of the two-nucleon transfer amplitudes have been obtained by fitting the experimental results for $^{40}Ca(^{14}C, ^{16}O)^{38}Ar$ and assuming them to be the same for all the processes. In fig. 7 we show this fitting to the two-nucleon transfer (b) and the result for the pair-exchange reaction (a). This result indicates that sequential two-nucleon transfer processes could account for half the magnitude of the experimental differential cross section.

TABLE 12

Cross sections for $^{40}Ca(^{14}C, ^{14}O)^{40}Ar$ reaction

		Wigner		Heisenberg		Wigner plus Heisenberg		Experiment	
J^π	E_x (MeV)	σ	σ_{rel}	σ	σ_{rel}	σ	σ_{rel}	$d\sigma/d\Omega$	$d\sigma_{rel}/d\Omega$
0^+	0.0	1.8	1	0.0044	1	1.8	1	6.5	1
2^+	1.46	0.0050	0.0027	1.9	426	1.9	1.06	5.0	0.77

Absolute and relative to the g.s. cross sections for the reaction $^{40}Ca(^{14}C, ^{14}O)^{40}Ar$ at the incident energy of 51 MeV. Columns 3 to 8 contain calculated angle-integrated cross sections. The experimental values are exctracted from fig. 2 of ref. [2]) for $\Theta_{c.m.} \simeq 15°$. The values of columns 3, 5 and 7 are in arbitrary units while those of column 9 are in μb/sr. The cross sections of column 7 are obtained assuming that the Wigner and Heisenberg processes add incoherently with equal strengths.

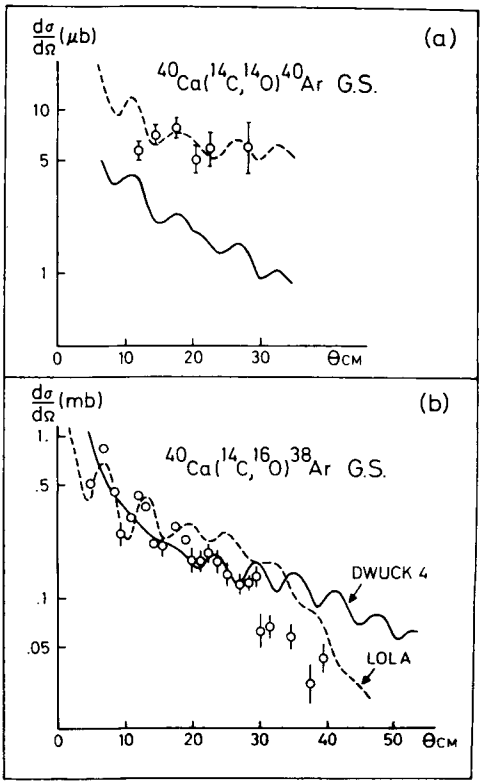

Fig. 7. (a) Differential cross sections calculated assuming two-step mechanisms (solid line) or direct arbitrarily normalized (dashed line). (b) Differential cross sections of the diproton transfer used to obtain the strengths of the processes entering the two-step description. Solid line: the calculation of the present work; dashed line: the calculation of ref. [2]). The experimental points in (a) and (b) are extracted from fig. 2 of ref. [2]).

4. Conclusions

In the present paper we have analyzed the pair-exchange reaction (^{14}C, ^{14}O) within the framework of direct, one-step mechanisms. Although coherent in principle, we have separately studied two different processes, that we have called "Wigner" and "Heisenberg", because they proceed through isospin independent and dependent terms, respectively, of the effective residual nuclear interaction.

In general, the results appear to be quite sensitive to nuclear structure considerations, apart from the angular momentum mismatches and Q-value effects. In particular, the interference between $S = 0$ and $S = 1$ channels is rather important for both processes. Therefore, for instance, the use of a configuration better than $(p_{\frac{1}{2}})^2$ for the dinucleons in the light system may lead to different and improved predictions. This will be specially true in the Ca case, where the $2^+/0^+$ relative ratios corresponding to Wigner and Heisenberg processes are very different. On the contrary, the results of the relative cross sections are qualitatively similar in the case of Po target for both processes. For this region there appears a distinct possibility to find states, like the two-proton pairing vibration or the α-vibration that have been sought for some time. Although, in principle, the reaction should also populate two-(particle-hole) states, the corresponding predicted cross sections are very small in both processes.

Appendix A

We derive the expressions (2) and (7) for the form factors, taking into account the assumptions (a)–(d).

A.1. WIGNER FORM FACTOR

A.1.1. Motion of the transferred dineutron in the residual target system B and in the projectile a. The states of the residual heavy system are expressed in terms of the dineutron and the states of the core C. These last ones are denoted by the quantum numbers (n'_C, J'_p, M_p), where J'_p is the angular momentum, M_p its projection and n'_C every additional one needed:

$$|B;\beta,J,M\rangle = \sum_{\substack{j_{1_n}\geqq j_{2_n}\\ n'_C J_n J'_p}} \langle B;\beta,J,M|[[[C^+_{j_{1_n}}C^+_{j_{2_n}}]^{J_n}|n'_C,J'_p\rangle]^J_M$$

$$\times\,[|j_{1_n},j_{2_n};J_n\rangle|n'_C,J'_p\rangle]^J_M. \qquad (A.1)$$

The label j_n represents the quantum numbers of the single-particle states (except

for their magnetic projection). The dinucleon states $(j_{1_n} j_{2_n}, J_n)$ can also be expressed in a representation with good spin S_n and total orbital angular momentum L_n. Finally, this last part is expressed in terms of the quantum numbers (n_n, l_n), describing the relative motion, and the c.m. quantum numbers $(N_n, \bar{L}_n)$, using a standard HO transformation. After some recouplings one obtains

$$|B; \beta, JM\rangle = \sum_{\substack{n'_C J_n J'_p \\ n_n N_n L_n \bar{L}_n S_n l_n \bar{l}_n I_n}} (2L_n+1)\sqrt{(2S_n+1)(2\bar{l}_n+1)(2J_n+1)(2I_n+1)}\,(-)^{l_n+L_n+\bar{l}_n+J_p+J}$$

$$\times \begin{Bmatrix} \bar{l}_n & J_n & \bar{L}_n \\ L_n & l_n & S_n \end{Bmatrix} \begin{Bmatrix} \bar{l}_n & \bar{L}_n & J_n \\ J'_p & J & I_n \end{Bmatrix} \eta(n_n, l_n, N_n, \bar{L}_n, L_n, S_n, J_n, n'_C)$$

$$\times [[|S_n\rangle|n_n, l_n\rangle]^{\bar{l}_n}[|N_n, \bar{L}_n\rangle|n'_C, J'_p\rangle]^{J_n}]^J_M, \tag{A.2}$$

where the "internal" dineutron coordinates are concentrated in the two terms that are coupled to $\bar{l}_n$. The factor η includes the nuclear structure information and is defined in eqs. (4) and (5).

The description of the projectile† $|a\rangle$ is simpler, since to a good approximation, it can be represented [14]) as a $[(p_{\frac{1}{2}})^2]^0$ configuration times the core $|c\rangle$ (which is the g.s. of ^{12}C). Moreover, the HO transformation brackets corresponding to two 0p particles coupled to $S_n(=0, 1)$ have the values

$$\langle n'_n, \bar{l}'_n; N'_n \bar{L}'_n; S_n|(0p)^2; S_n\rangle = \delta_{\bar{l}'_n S_n}\delta_{\bar{L}'_n S_n}\delta_{N'_n,(1-n'_n-S_n)}\frac{(-)^{n'_n}}{\sqrt{2-S_n}}. \tag{A.3}$$

Using these values, the projectile $|a\rangle$ is given by

$$|a\rangle = |(0p_{\frac{1}{2}})^2; 0\rangle|c\rangle$$

$$= \sqrt{2}\sum_{n'_n N_n S'_n} (-)^{n_n+S_n}\sqrt{\frac{2S'_n+1}{2-S'_n}} \begin{Bmatrix} 1 & 1 & S'_n \\ \frac{1}{2} & \frac{1}{2} & \frac{1}{2} \end{Bmatrix}$$

$$\times [[|S'_n\rangle|n'_n, S'_n\rangle]^{S'_n}|(1-n'_n-S'_n), S'_n\rangle]^0|c\rangle, \tag{A.4}$$

† The $[(p_{\frac{1}{2}})^2]^0$ dinucleon state in the light systems is an assumption not well supported by the calculations of Cohen and Kurath [14]). The use of a better wave function would amount to introducing excited states of the core $|c\rangle$ (and keeping track of them in the integration in the internal variables of ^{12}C) and the component (0, 2) of the c.m. wave function (N, L) (in addition to (0, 0), (1, 0) and (0, 1)). Although this is quite possible to perform, we feel that the $[(p_{\frac{1}{2}})^2]^0$ simplication is sufficiently good within the scope of the present study, since it provides a reasonable radial c.m. wave function in order to construct the form factor. Similar considerations are made for the ejectile.

where as in (A.2) the internal dineutron degrees of freedom are coupled first and the state $|(1-n'_n-S'_n), S'_n\rangle$ represents the motion of the centre of mass. Either n'_n and S'_n can be zero or one, and the radial quantum number $(1-n'_n-S'_n)$ must be non-negative.

A.1.2. Integration over the internal dineutron coordinates.

$$\begin{aligned}\langle a|B;\,\beta,\,JM\rangle = \sqrt{2}\sum_{n'_C J_n J'_p}(-)^{J+J'_p}\sqrt{2J_n+1}\\ \times \sum_{\substack{n_n N_n n'_p \\ L_n S_n \bar{L}_n I_n}}(-)^{L_n+S_n+n'_n}\frac{(2L_n+1)(2S_n+1)\sqrt{2I_n+1}}{\sqrt{2-S_n}}\\ \times \begin{Bmatrix}1 & 1 & S_n\\ \frac{1}{2} & \frac{1}{2} & \frac{1}{2}\end{Bmatrix}\begin{Bmatrix}S_n & S_n & S_n\\ L_n & J_n & \bar{L}_n\end{Bmatrix}\begin{Bmatrix}S_n & \bar{L}_n & J_n\\ J'_p & J & I_n\end{Bmatrix}\\ \times \langle n'_n,\,S_n|n_n,\,S_n\rangle\eta(n_n,\,S_n,\,N_n,\,\bar{L}_n,\,L_n,\,S_n,\,n'_c)\\ \times \langle c|[\langle(1-n'_n-S_n),\,S_n|[|N_n,\,\bar{L}_n\rangle|n'_c,\,J'_p\rangle]^{I_n}]^{J}_{M}. \qquad (A.5)\end{aligned}$$

A.1.3. Integration over the internal diproton coordinates. The corresponding expression is similar to (A.5) with $J = 0$ and $J_n = J'_p = J_p$:

$$\begin{aligned}\langle b|A\rangle = \sqrt{2}\sum_{n_C J_p}\sum_{\substack{n_p N_p n'_p \\ L_p S_p}}(-)^{L_p+\bar{L}_p+n'_p}\frac{(2L_p+1)(2S_p+1)}{\sqrt{2-S_p}}\\ \times \begin{Bmatrix}1 & 1 & S_p\\ \frac{1}{2} & \frac{1}{2} & \frac{1}{2}\end{Bmatrix}\begin{Bmatrix}S_p & S_p & S_p\\ L_p & J_p & \bar{L}_p\end{Bmatrix}\langle n'_p,\,S_p|n_p,\,S_p\rangle\\ \times \eta(n_p,\,S_p,\,N_p,\,\bar{L}_p,\,L_p,\,S_p,\,n_c)\\ \times \langle c|[\langle(1-n'_p-S_p),\,S_p|[[N_p\bar{L}_p\rangle|n_C J_p\rangle]^{S_p}\rangle]^{0}. \qquad (A.6)\end{aligned}$$

A.1.4. Integration over the internal coordinates of the core C and the core c.

$$\begin{aligned}\langle c|[\langle N'_n,\,S_n|[|N_n,\,\bar{L}_n\rangle|n'_C,\,J'_p\rangle]^{I_n}]^{J'}_{M}\,\langle c|[\langle N'_p,\,S_p|[|N_p,\,\bar{L}_p\rangle|n_C,\,J_p\rangle]^{S_p}]^{0}\\ = \delta_{n'_C n_C}\delta_{J_p J'_p}(-)^{J+M+J_p}\sum_{I_p}(-)^{\bar{L}_n+S_p+I_p}\sqrt{2I_p+1}\begin{Bmatrix}I_n & \bar{L}_n & J_p\\ \bar{L}_p & S_p & I_p\end{Bmatrix}\\ \times[\Phi_{N'_n S_n}(\boldsymbol{r}_n-\boldsymbol{R})[\Phi_{N'_p S_p}(\boldsymbol{r}_p-\boldsymbol{R})[\Phi_{N_n\bar{L}_n}(\boldsymbol{r}_n)\Phi_{N_p\bar{L}_p}(\boldsymbol{r}_p)]^{I_p}]^{I_n}]^{J}_{-M}. \qquad (A.7)\end{aligned}$$

Here we have explicitly introduced the wave functions of the c.m. dineutron and diproton coordinates. The frame of reference is centered at the c.m. of the large core C. The coordinate of core c is denoted by R (assumption (b)).

A.1.5. Integration over the c.m. coordinates of the diproton and dineutron. Finally, the form factor is obtained from the expression (assumption (a)):

$$\langle b|\langle B;\beta,J,M|V(|\boldsymbol{r}_n-\boldsymbol{r}_p|)|A\rangle|a\rangle$$

$$= 2(-)^M \sum_{n_C,J_n,J_p} \sqrt{2J_n+1} \sum_{\substack{n_nN_nn'_nS_nL_n\bar{L}_nI_n \\ n_pN_pn'_pS_pL_p\bar{L}_pI_p}} (-)^{I_p} \begin{Bmatrix} I_n & \bar{L}_n & J_p \\ \bar{L}_p & S_p & I_p \end{Bmatrix} \begin{Bmatrix} S_n & \bar{L}_n & J_n \\ J_p & J & I_n \end{Bmatrix}$$

$$\times \int d\boldsymbol{r}_n d\boldsymbol{r}_p V(|\boldsymbol{r}_n-\boldsymbol{r}_p|)[\Phi_{(1-n'_n-S_n),S_n}(\boldsymbol{r}_n-\boldsymbol{R})[\Phi_{(1-n'_p-S_p),S_p}(\boldsymbol{r}_p-\boldsymbol{R})$$

$$[\Phi_{N_n\bar{L}_n}(\boldsymbol{r}_n)\Phi_{N_p\bar{L}_p}(\boldsymbol{r}_p)]^{I_p}]^{I_n}]^{J}_{-M}$$

$$\times \prod_{z=n,p} (-)^{n'_z+L_z+\bar{L}_z+S_z} \frac{(2L_z+1)(2S_z+1)\sqrt{2I_z+1}}{\sqrt{2-S_z}}$$

$$\times \begin{Bmatrix} 1 & 1 & S_z \\ \frac{1}{2} & \frac{1}{2} & 2 \end{Bmatrix} \begin{Bmatrix} S_z & S_z & S_z \\ L_z & J_z & \bar{L}_z \end{Bmatrix} \eta(n_z,S_z,N_z,L_z,\bar{L}_z,S_z,J_z,n_C)$$

$$\times \langle n'_z,S_z|n_z,S_z\rangle. \tag{A.8}$$

The integral in (A.8) is evaluated using an approximation of the Buttle-Goldfarb type, since the more exact calculation is not justified at this stage of the study of the pair-exchange processes (assumption (c)).

This assumption is based on the fact that any wave function Φ_{nl} of (A.8) carries, apart from polynomials depending on n and l, a factor decaying exponentially with the distance between the dinucleon and the cores C or c. Therefore the products $\Phi(\boldsymbol{r})\Phi(\boldsymbol{r}-\boldsymbol{R})$ attain their largest value when both $\boldsymbol{r}$ and $\boldsymbol{r}-\boldsymbol{R}$ lie along the line joining the two cores (i.e. along $\boldsymbol{R}$, fig. 1a). The assumption is then made that only these extremal values contribute to the integral of (A.8), a result that can be obtained by writing

$$V(|\boldsymbol{r}_n-\boldsymbol{r}_p|) = \frac{V(|\boldsymbol{r}_n-\boldsymbol{r}_p|)}{r_n^2r_p^2} \delta(\Omega_n-\Omega_R)\delta(\Omega_p-\Omega_R), \tag{A.9}$$

where Ω_n, Ω_p and Ω_R indicate the direction (Θ_n,φ_n), (Θ_p,φ_p) and (Θ_R,φ_R) respectively. The integral of (A.8) becomes

$$[Y_{S_n}(\Omega_R)[Y_{S_p}(\Omega_R)[Y_{\bar{L}_n}(\Omega_R)Y_{\bar{L}_p}(\Omega_R)]^{I_p}]^{I_n}]^{J}_{-M}$$

$$\times \int d\boldsymbol{r}_n d\boldsymbol{r}_p V(|\boldsymbol{r}_n-\boldsymbol{r}_p|)\Psi_{N_n,\bar{L}_n}(\boldsymbol{r}_n)\Psi_{N_p,\bar{L}_p}(\boldsymbol{r}_p)\Psi_{(1-n'_n-S_n),S_n}(|\boldsymbol{r}-\boldsymbol{R}|)\Psi_{(1-n'_p-S_p),S_p}(|\boldsymbol{r}_p-\boldsymbol{R}|), \tag{A.10}$$

which can also be written as

$$\frac{Y_{J,-M}(\Omega_R)}{(4\pi)^{\frac{1}{2}}}\, i^{S_n-S_p+\bar{L}_p+\bar{L}_n-J}\sqrt{\frac{(2\bar{L}_n+1)(2\bar{L}_p+1)(2S_n+1)(2S_p+1)}{2I_n+1}}$$
$$\times\langle JS_n00|I_n0\rangle\langle I_pS_p00|I_n0\rangle\langle\bar{L}_n\bar{L}_p00|I_p0\rangle$$
$$\times\int dr_n dr_p \Psi_{(1-n_n'-S_n),S_n}(|r_n-R|)\Psi_{(1-n_p'-S_p),S_p}(|r_p-R|)\Psi_{N_n,\bar{L}_n}(r_n)\Psi_{N_p,\bar{L}_p}(r_p). \quad (A.11)$$

The replacement of (A.11) in (A.8) and the application of standard sum rules for the 6-j symbol, yield

$$\langle b|\langle B;\ \beta,\ J,\ M|V(|r_n-r_p|)|A\rangle|a\rangle = \frac{-i^J}{4\pi^{\frac{1}{2}}}\frac{Y^*_{JM}(\Omega_R)}{\sqrt{2J+1}}\sum_{\substack{n_C,J_n,J_p\\ n_nN_nn_n'S_nL_n\bar{L}_n\\ n_pN_pn_p'S_pL_p\bar{L}_p}}\langle J_nJ_p00|J0\rangle$$
$$\times\int dr_n dr_p V(|r_n-r_p|)\Psi^{(B,\beta,J,M)}_{N_n,\bar{L}_n}(r_n)\Psi^{(A)}_{N_p,\bar{L}_p}(r_p)\Psi^{(^{14}C)}_{(1-n_n-S_n),S_n}(|r_n-R|)\Psi^{(^{14}O)}_{(1-n_p'-S_p),S_p}(|r_p-R|)$$
$$\times\prod_{z=n,p} i^{L_z-S_z}(-)^{N_z+L_z+n_z'}(2L_z+1)\sqrt{\frac{(2S_z+1)^3(2\bar{L}_z+1)}{(2-S_z)}}\langle\bar{L}_zS_z00|J_z0\rangle$$
$$\times\begin{Bmatrix}1&1&S_z\\ \frac{1}{2}&\frac{1}{2}&\frac{1}{2}\end{Bmatrix}\begin{Bmatrix}S_z&S_z&S_z\\ L_z&\bar{L}_z&J_z\end{Bmatrix}\eta(n_z,\ S_z,\ N_z,\ \bar{L}_z,\ L_z,\ S_z,\ J_z,\ n_C). \quad (A.12)$$

The application of assumption (d) concerning the short-range nature of the interaction, yields expression (2).

A.2. HEISENBERG FORM FACTOR

A.2.1. Initial and final states. The states of the residual nucleus and of the projectile are expressed as in (A.2) and (A.4), respectively. Similar expressions hold for the target and projectile. However, we made a slight change in the notation, since in Heisenberg processes there is a dinucleon T associated with the target (residual) system and another dinucleon t associated with the projectile (ejectile). Therefore,

$$|{}^a_b\rangle = \sqrt{2}\sum_{n_tN_tS_t}(-)^{n_t+S_t}\sqrt{\frac{2S_t+1}{2-S_t}}\begin{Bmatrix}1&1&S_t\\ \frac{1}{2}&\frac{1}{2}&\frac{1}{2}\end{Bmatrix}$$
$$\times[[|S_t\rangle|n_t,\ S_t\rangle]^{S_t}|(1-n_t-S_t),\ S_t\rangle]^0|\pm\rangle|c\rangle, \quad (A.13)$$

$$|A\rangle = \sum_{\substack{n_C J_p n_T S_T l_T \\ N_p L_p \bar{L}_p I_p}} (-)^{l_T + L_p + I_p} (2L_p + 1) \sqrt{2S_T + 1} \begin{Bmatrix} I_p & J_p & \bar{L}_p \\ L_p & l_T & S_T \end{Bmatrix}$$

$$\times \eta(n_T, l_T, N_p, \bar{L}_p, L_p, S_T, J_p, n_C)$$

$$\times [[|S_T\rangle|n_T, l_T\rangle]^{I_p}[|N_T, \bar{L}_p\rangle|n_C J_p\rangle]^{I_p}]^0|-\rangle,$$

$$|B\rangle = \sum_{\substack{n_C J_p n_T S_T l_T \\ N_n L_n \bar{L}_n I_p I_n}} (-)^{l_T + L_n + I_p + J_p + J} (2L_n + 1) \sqrt{(2S_T + 1)(2I_p + 1)(2J_n + 1)(2I_n + 1)}$$

$$\times \begin{Bmatrix} I_p & J_n & \bar{L}_n \\ L_n & l_T & S_T \end{Bmatrix} \begin{Bmatrix} I_p & \bar{L}_n & J_n \\ J_p & J & I_n \end{Bmatrix} \eta(n_T, l_T, N_n, \bar{L}_n, L_n, S_T, J_n, n_C)$$

$$\times [[|S_T\rangle|n_T, l_T\rangle]^{I_p}[|N_n, \bar{L}_n\rangle|n_C, J_p\rangle]^{J_n}]^J_M|+\rangle. \tag{A.14}$$

The $|+\rangle(|-\rangle)$ isospin symbol denotes a dineutron (diproton).

A.2.2. Integration over the internal coordinates of the dinucleon t and the core c, and of the dinucleon T and the core C.

$$\langle b|\tau_t|a\rangle = 2 \sum_{n_t S_t} \sqrt{\frac{2S_t + 1}{2 - S_t}} \begin{Bmatrix} 1 & 1 & S_t \\ \frac{1}{2} & \frac{1}{2} & \frac{1}{2} \end{Bmatrix}^2$$

$$\times [\Phi^{(^{14}C)}_{(1-n_t-S_t),S_t}(\boldsymbol{r}_t - \boldsymbol{R})\Phi^{(^{14}O)}_{(1-n_t-S_t),S_t}(\boldsymbol{r}_t - \boldsymbol{R})]^0, \tag{A.15}$$

$$\langle B; J, M|\tau_T|A\rangle = (-)^{J+M} \sum_{\substack{n_C J_n J_p S_T n_T l_T \\ N_p L_p \bar{L}_p N_n L_n \bar{L}_n}} (-)^{J_p + \bar{L}_p + l_T + S_T}$$

$$\times (2L_n + 1)(2L_p + 1)(2S_T + 1)\sqrt{(2J_n + 1)(2J_p + 1)}$$

$$\times \begin{Bmatrix} J_n & S_T & L_n \\ L_p & J & J_p \end{Bmatrix} \begin{Bmatrix} \bar{L}_n & l_T & L_n \\ L_p & J & L_p \end{Bmatrix}$$

$$\times \eta(n_T, l_T, N_n, L_n, S_T, J_n, \gamma_C)\eta(n_T, l_T, N_p, \bar{L}_p, S_T, J_p, \gamma_C)$$

$$\times [\Phi^{(A)}_{N_n, \bar{L}_n}(\boldsymbol{r}_T)\Phi^{(B,JM)}_{N_p, \bar{L}_p}(\boldsymbol{r}_T)]^J_{-M}. \tag{A.16}$$

Here we have used

$$\langle -|\tau_t|+\rangle = \langle +|\tau_T|-\rangle = 1. \tag{A.17}$$

A.2.3. Integration for the c.m. coordinate of the dinucleon T and t.

$$\langle b|\langle B(JM)|V(|\boldsymbol{r}_t-\boldsymbol{r}_T|)\tau_t\cdot\tau_T|A\rangle|a\rangle$$

$$= -2(-)^{J+M}\sum_{n_C J_n J_p}\sum_{\substack{S_t n_t S_T n_T l_T \\ N_p \bar{L}_p L_p N_n L_n \bar{L}_n}}(-)^{J_p+\bar{L}_p+l_T+S_T}(2S_T+1)\sqrt{\frac{2S_t+1}{2-S_t}}$$

$$\times \begin{Bmatrix} 1 & 1 & S_T \\ \frac{1}{2} & \frac{1}{2} & \frac{1}{2} \end{Bmatrix}^2 \begin{Bmatrix} J_n & S_T & L_n \\ L_p & J & J_p \end{Bmatrix} \begin{Bmatrix} \bar{L}_n & l_T & L_n \\ L_p & \bar{J} & \bar{L}_p \end{Bmatrix}$$

$$\times \int d\boldsymbol{r}_t d\boldsymbol{r}_T V(|\boldsymbol{r}_t-\boldsymbol{r}_T|)\left[\Phi^{(^{14}C)}_{(1-n_t-S_t),S_t}(\boldsymbol{r}_t-\boldsymbol{R})\Phi^{(^{14}O)}_{(1-n_t-S_t),S_t}(\boldsymbol{r}_t-\boldsymbol{R})\right]^0\left[\Phi^{(B)}_{N_n,\bar{L}_n}(\boldsymbol{r}_T)\Phi^{(A)}_{N_p,\bar{L}_p}(\boldsymbol{r}_T)\right]^J_{-M}$$

$$\times \prod_{z=n,p}(2L_z+1)\eta(n_T, l_T, N_z, \bar{L}_z, L_z, S_T, J_z, n_C)$$

$$= \frac{-i^J}{4\pi^{\frac{1}{2}}(2J+1)}Y^*_{JM}(\Omega_R)$$

$$\times \sum_{n_t S_t}\sqrt{\frac{2S_t+1}{2-S_t}}\begin{Bmatrix} 1 & 1 & S_t \\ \frac{1}{2} & \frac{1}{2} & \frac{1}{2} \end{Bmatrix}^2$$

$$\times \sum_{N_n \bar{L}_n N_p \bar{L}_p} i^{\bar{L}_n+\bar{L}_p}\langle \bar{L}_n \bar{L}_p 00|J0\rangle$$

$$\times \int d\boldsymbol{r}_t d\boldsymbol{r}_T V(|\boldsymbol{r}_t-\boldsymbol{r}_T|)\,\Psi^{(B,J)}_{N_n\bar{L}_n}(\boldsymbol{r}_T)\Psi^{(A)}_{N_p\bar{L}_p}(\boldsymbol{r}_T)\Psi^{(^{14}C)}_{(1-n_t-S_t)S_t}\Psi^{(^{14}O)}_{(1-n_t-S_t)S_t}(|\boldsymbol{r}_t-\boldsymbol{R}|)$$

$$\times \sum_{\substack{L_n \bar{L}_p J_n J_p \\ n_T S_T l_T n_C}}(-)^{J_p+\bar{L}_n+S_T+l_T}(2S_T+1)\begin{Bmatrix} J_n & S_T & L_n \\ L_p & J & J_p \end{Bmatrix}\begin{Bmatrix} \bar{L}_n & l_T & L_n \\ L_p & J & \bar{L}_p \end{Bmatrix}$$

$$\times \prod_{z=n,p}(2L_z+1)\sqrt{(2J_z+1)(2L_z+1)}\,\eta(n_T, l_T, N_z, \bar{L}_z, L_z, S_T, J_z, n_C). \tag{A.18}$$

The last expression is obtained through application of the Buttle-Goldfarb approximation. The final expression (7) is obtained by making the short-range approximation for the interaction.

Appendix B

THE DESCRIPTION OF STATES AROUND ^{208}Pb

The concept of elementary excitations or elementary building blocks has proven to be especially successful in the description of states around ^{208}Pb. In this paper we use these excitations, which are represented by pairing and particle-hole bosons. They carry the quantum numbers (α, z, J, M, n) where the transfer number α

equals a for an addition pairing phonon, r for a removal pairing phonon and 0 for a particle-hole phonon. The symbol $z(=\mathrm{n},\ \mathrm{p})$ denotes a neutron or a proton component and J and M are angular momentum labels. The number n distinguishes between phonons carrying the same other quantum numbers and is omitted hereafter. As an example, the 2.16 MeV, $J=3$ state in ^{208}Pb is obtained acting with the boson creation Γ^+ on the ground state $|0\rangle$:

$$|^{208}\mathrm{Pb};\ 2.61\ \mathrm{MeV}\rangle = |(\mathrm{ph}),\ J=3,\ M\rangle = \sum_{z=\mathrm{n,p}} \Gamma^+(0,\ z,\ 3,\ M)|0\rangle. \tag{B.1}$$

The target $|\mathrm{A}\rangle$ (i.e. the g.s. of ^{208}Pb) is formed with two pairing phonons:

$$|\mathrm{A}\rangle = \Gamma^+(\mathrm{r},\ \mathrm{n},\ 0,\ 0)\Gamma^+(\mathrm{a},\ \mathrm{p},\ 0,\ 0)|0\rangle. \tag{B.2}$$

In the TDA, the boson operators Γ^+, Γ are transcribed as linear combinations of a pair of fermion operators:

$$\begin{aligned}
\Gamma^+(\mathrm{a},\ z,\ J,\ M) &= \sum_{k_{z_1} \leqq k_{z_2}} \lambda(\mathrm{a},\ z,\ J;\ k_{z_1},\ k_{z_2})[C^+_{k_{z1}}C^+_{k_{z2}}]^J_M/\sqrt{1+\delta_{1,2}},\\
\Gamma^+(\mathrm{r},\ z,\ J,\ M) &= \sum_{i_{z_1} \leqq i_{z_2}} \lambda(\mathrm{r},\ z,\ J;\ i_{z_1},\ i_{z_2})[C_{i_{z1}}C_{i_{z2}}]^J_M/\sqrt{1+\delta_{1,2}},\\
\Gamma^+(0,\ z,\ J,\ M) &= \sum_{k_z,i_z} \lambda(0,\ z,\ J;\ k_z,\ i_z)[C^+_{k_z}C_{i_z}]^J_M.
\end{aligned} \tag{B.3}$$

Here k denotes all the single-particle labels for empty states; similarly i, for occupied states. For the pairing operators, the inverse relations to (B.3) relate the pair creation $[C^+_{j_1}C^+_{j_2}]^J_M$ to the boson operators

$$\begin{aligned}
[C^+_{k_1}C^+_{k_2}]^J_M/\sqrt{1+\delta_{1,2}} &= \lambda(\mathrm{a},\ z,\ J;\ k_1,\ k_2)\Gamma^+(\mathrm{a},\ z,\ J,\ M) \qquad (k_1 \geqq k_2),\\
[C^+_{i_1}C^+_{i_2}]^J_M/\sqrt{1+\delta_{1,2}} &= \lambda(\mathrm{r},\ z,\ J;\ i_1,\ i_2)\Gamma(\mathrm{r},\ z,\ J,\ -M) \qquad (i_1 \geqq i_2).
\end{aligned} \tag{B.4}$$

The operators $[C^+_k C^+_i]^J$ are expressed in terms of two-phonon operators:

$$\begin{aligned}
[C^+_k C^+_i]^J_M = &-\sqrt{2}\lambda(\mathrm{r},\tau,0;i,i)\lambda(0,z,J;k,i)\frac{1}{\sqrt{2i+1}}\Gamma^+(0,z,J,M)\Gamma(\mathrm{r},z,0,0)\\
&+\sqrt{2}\lambda(\mathrm{a},z,0;k,k)\lambda(0,z,J;k,i)\frac{(-)^{J-M}}{\sqrt{2k+1}}\Gamma(0,z,J,-M)\Gamma^+(\mathrm{a},z,0,0),
\end{aligned} \tag{B.5}$$

where it has been assumed that the pairing bosons carry zero angular momentum.

Using expressions (B.2) for the target $|A\rangle$ and (B.4) and (B.5) for the pair creation operators, we easily calculate the matrix elements entering in the structure factors η, (4) and (5). We order the states to be populated in the residual system according to the number of particle-hole excitations.

(*i*) *Ground-state transition.* The dineutron fills the two holes in the closed shell while simultaneously the two protons are removed from the upper shell. Therefore, the only intermediate core state is the g.s. of ^{206}Pb, $|r, n, 0\rangle$ and the matrix elements entering in the structure factors are the amplitudes λ:

$$\langle 0|\sqrt{\tfrac{1}{2}}[C_i^+ C_i^+]^0|r, n, 0\rangle = -\lambda(r, n, 0; i, i), \tag{B.6}$$

$$\langle A|\sqrt{\tfrac{1}{2}}[C_k^+ C_k^+]|r, n, 0\rangle = \lambda(a, p, 0; k, k). \tag{B.7}$$

(*ii*) *Particle-hole states.* The population of states $|0, z, J\rangle$ can be made via two paths: in the first one, protons are picked up as in the reaction populating the g.s., thus yielding the same intermediate states $|r, n, 0\rangle$ and the same matrix elements (B.7). Simultaneously, one of the neutrons fills a hole while the second one occupies a particle state:

$$\langle (ph), J|[C_k^+ C_i^+]^J|r, n, 0\rangle = -\sqrt{2}\lambda(r, n, 0; i, i)\lambda(0, n, J; k, i)/\sqrt{2i+1}. \tag{B.8}$$

In the second path, the two neutron-hole states are filled as in the population of the g.s. (matrix element (B.6)) and the captured diproton leaves a particle-hole proton pair. Thus, the intermediate state is a proton particle-hole excitation in ^{206}Pb:

$$\langle A|[[C_k^+ C_i^+]^J|(r, n, 0)(0, p, J)\rangle]^0 \frac{1}{\sqrt{2J+1}}$$

$$= \sqrt{2}\lambda(a, p, 0; k, k)\lambda(0, p, J; k, i)/\sqrt{2k+1}. \tag{B.9}$$

The processes along the two paths add coherently.

(*iii*) *Two particle-hole states.* The possibility of reaching these states through relatively enhanced cross sections constitutes an attractive feature of pair-exchange reactions. Two different states of this type are considered, namely:

(*a*) *States belonging to the family of pairing vibrations.* If a neutron two-phonon state is excited, the protons are captured as for the population of the g.s. (B.7). Simultaneously the two neutrons are put in the empty states, as in ^{210}Pb:

$$\langle (r, n, 0)(a, n, J)|\frac{[C_{k_1}^+ C_{k_2}^+]^J}{\sqrt{1+\delta_{1,2}}}|r, n, 0\rangle = \lambda(a, n, J; k_1, k_2). \tag{B.10}$$

Similarly for the population of a proton two-phonon state. In this case, the intermediate state is the proton two-phonon pairing state in ^{206}Pb:

$$\langle A|\frac{[C^+_{i_1}C^+_{i_2}]^J_M}{\sqrt{1+\delta_{1,2}}}|(r, n, 0)(a, p, 0)(r, p, J)\rangle = -\lambda(r, p, J; i_1, i_2\rangle, \tag{B.11}$$

while the neutron matrix element is always (B.6).

(*b*) *Two one- (particle-hole) phonon states* $[|(ph), J_1\rangle|(ph), J_2\rangle]^J$. Again, two possible paths are present. In the first one, the substraction of a diproton creates a particle-hole state in ^{206}Pb carrying angular momentum J_2; the addition of a dineutron creates a second particle-hole pair with angular momentum J_1:

$$\langle[(ph)J_1, (ph)J_2]^J|[[C^+_{k_n}C^+_{i_n}]^{J_1}|(r, n, 0)(0, p, J_2)\rangle]^J$$
$$= \sqrt{2-\delta_{12}}\ \lambda(r, n, 0; i_n, i_n)\lambda(0, n, J_2; k_n, i_n)/\sqrt{2i_n+1}, \tag{B.12}$$

$$\langle A|[[C^+_{k_p}C^+_{i_p}]^{J_2}|(r, n, 0)(0, p, J_2)\rangle]^0 \frac{1}{\sqrt{2J_2+1}}$$
$$= \sqrt{2}\,\lambda(a, p, 0; k_p, k_p)\lambda(0, p, J_2; k_p, i_p)/\sqrt{2k_p+1}. \tag{B.13}$$

In the second path, the neutron particle-hole excitation carries angular momentum J_2, while the proton core carries angular momentum J_1:

$$\langle[(ph)J_1, (ph)J_2]^J|[[C^+_{k_n}C^+_{i_n}]^{J_2}|(r, n, 0)(0, p, J_1)\rangle]^J$$
$$= -\sqrt{2-\delta_{1,2}}(-)^{J_1+J_2-J}\lambda(r, n, 0; i_n, i_n)\lambda(0, n, J_1; k_n, i_n)/\sqrt{2i_n+1}, \tag{B.14}$$

$$\langle A|[[C^+_{k_p}C^+_{i_p}]^{J_1}|(r, n, 0)(0, p, J_1)\rangle]^0 \frac{1}{\sqrt{2J_1+1}}$$
$$= \sqrt{2}\lambda(a, p, 0; k_p, k_p)\lambda(0, p, J_1; k_p, i_p)/\sqrt{2k_p+1}. \tag{B.15}$$

(*c*) *Three particle-hole states* $|r, n, 0\rangle$ $[|a, n, J_1\rangle|(p, h), J_2\rangle]^J$. For instance, the stripped dineutron is put in states above the Fermi sea while the capture diproton creates a particle-hole excitation. Thus the proton matrix element is given by (B.13) while the neutron one by (B.11) with $J = J_1$.

(*d*) *Four particle-hole states* $|r, n, 0\rangle|a, p, 0\rangle[|a, n, J_n\rangle|r, p, J_p\rangle]^J$. The stripped dineutron occupies empty states; the captured diproton leaves two holes in the closed shells. The neutron matrix element is given by (B.10), while the proton matrix elements, by (B.11).

Therefore, the calculation of the matrix elements entering the structure factors

TABLE 13

The single-particle energies ε_j (in MeV)

	Neutrons	Protons		Neutrons	Protons
$d_{3/2}$	4.24		$p_{3/2}$	−2.61	5.24
$g_{7/2}$	4.20		$i_{13/2}$	−3.33	3.73
$s_{1/2}$	3.74		$f_{7/2}$	−4.04	3.02
$d_{5/2}$	5.27		$h_{9/2}$	−5.17	2.13
$j_{15/2}$	3.13		$s_{1/2}$		−2.13
$i_{11/2}$	2.48		$d_{3/2}$		−2.48
$g_{9/2}$	1.70		$h_{11/2}$		−3.47
$p_{1/2}$	−1.70	5.75	$d_{5/2}$		−3.80
$f_{5/2}$	−2.27	4.94	$g_{7/2}$		−5.61

η [eqs. (5) and (6)] is performed through a systematic use of the amplitudes of the elementary excitations [eq. (B.3)]. There are many calculations of these amplitudes, using different residual interactions. All of them yield rather similar values of λ, at least for the collective states. Thus, we use the results of a surface delta interaction in a TDA calculation †:

$$\lambda(\alpha, z, J; j_1, j_2) = N_J(-)^{n_1+n_2}\langle j_1 \| Y_\lambda \| j_2 \rangle / (\varepsilon_{j_1} + \varepsilon_{j_2} - \omega_J). \tag{B.16}$$

Here ω_J is the experimental phonon energy and N_J is a normalization constant. The single-particle energies ε_j and the phonon energies are given in tables 13 and 14, respectively.

TABLE 14

The phonon frequencies ω_J

α	z	J	ω_J (MeV)
r	n	0	−2.76
a	n	0	2.16
a	n	2	2.96
r	p	0	−0.321
r	p	2	−4.22
a	p	0	2.60
0	n, p	3	2.61
0	n, p	5	3.20

† The phase $(n)^{n_1+n_2}$ reflects the convention on the radial wave function which has the sign $(-)^n$ as $r \to \infty$.

In order to simplify the calculation of the factors η, the state of different parity in each shell has been replaced by the missing state in the same shell. For instance, the $i_{\frac{13}{2}}$ state in the neutron filled shell is replaced by the $h_{\frac{11}{2}}$. Thus all states of the same shell correspond to the same harmonic oscillator shell and the quantum number

$$\bar{N} = 2n_1 + l_1 + 2n_2 + l_2 \tag{B.17}$$

is constant for any path discussed above. However, only the $(j_1, j_2)^J$ combinations allowed by the original parity selection rules are admitted in (B.16).

References

1) G. R. Burleson, Los Alamos Scientific Laboratory Report No. LA-8303-C, (1980, unpublished), p. 195;
E. Oset, D. Strottman and G. E. Brown, Phys. Lett. **73B** (1978) 393
2) D. M. Drake, J. D. Moses, J. C. Peng, N. Stein and J. W. Sunier, Phys. Rev. Lett. **45** (1980) 1765
3) H. H. K. Tang and J. S. Vaagen, J. Math. Phys. **22** (1981) 785
4) P. D. Kunz, unpublished
5) K. S. Low and T. Tamura, Phys. Lett. **48B** (1974) 285
6) S. C. Pieper *et al.*, Phys. Rev. **C18** (1978) 180
7) M. C. Lemaire, M. C. Mermaz, H. Sztark and A. Cunsolo, Phys. Rev. **C10** (1974) 1103
8) W. Nörenberg and H. A. Weidenmüller, Introduction to the theory of heavy-ion collisions, Lectures Notes in Physics (Springer, Berlin, 1976)
9) D. R. Bes, O. Dragún, E. E. Maqueda and R. J. Liotta, Phys. Lett. **106B** (1981) 1
10) J. H. Bjerregaard, O. Hansen, O. Nathan and S. Hinds, Nucl. Phys. **89** (1966) 337
11) G. Igo, P. Barnes and E. Flynn, Ann. of Phys. **66** (1971) 60
12) J. R. Southon, A. R. Poletti and D. J. Beale, Nucl. Phys. **A267** (1976) 263
13) P. D. Kunz, (unpublished)
14) S. Cohen and D. Kurath, Nucl. Phys. **141** (1970) 145